

Potential Flow Calculations of Axisymmetric Ducted Wind Turbines

Sheila Widnall

Massachusetts Institute of Technology

July 2009

Introduction

An incompressible potential-flow vortex method has been constructed to analyze the flow field of a ducted wind turbine following that outlined by Lewis (1991). Attention is paid to balancing the momentum change in the flow to the total longitudinal forces acting on the duct-turbine combination: the pressure force on the actuator disk plus the pressure forces acting on the duct, which typically includes a negative component of drag due to high leading-edge suction. These forces are shown to balance the momentum changes in the flow, resulting in a model for power output from a ducted wind turbine over a wide range of pressure changes across the actuator disk. The results are compared to the Betz actuator disk model and it is shown that the maximum power output from a ducted turbine occurs at a lower value of pressure drop/momentum extraction than that for a bare turbine.

In this method, vortex panels are used to define the shape of the duct and to account for the flow changes due to the pressure drop across the turbine disk. It may seem surprising that potential flow can be used to describe the flow of a ducted wind turbine, but under the assumption of uniform changes in static and stagnation pressure across the turbine disk, as is done in the Betz model, both regions of the flow have a potential function. The velocity field, which is irrotational, is unchanged across the actuator disk. The two regions of flow are defined by the stagnation pressure change across the actuator disk and by the cylindrical vortex sheet that originates from the trailing edge of the duct as a result of the pressure changes across the disk.

In experiments in which the actuator disk is replaced by a uniform screen, the change in stagnation pressure is not likely to be constant across the actuator disk due to the non-uniform velocity at the disk entry. This calls into question the use of screens to represent an actuator disk across which the change in stagnation pressure is assumed to be constant. However, these errors are of the same order as the application of actuator disk theory itself to a problem as complex as a wind turbine with a finite or an infinite number of blades. In any case this potential flow model should be considered to be a descendent of the Betz model and other similar analysis of ducted propellers and should give useful insights into the operation of ducted wind turbines.

The advantages of such a simplified model are that basic questions can be investigated without the complexity of a full CFD simulation: basic questions such as the momentum balance in the flow; the forces acting on the duct; the role of the Kutta condition in comparison to its usual form for an airfoil in a uniform potential

flow; the interaction between the external and the internal flows, and the circulation about the airfoil/duct. This model moves beyond the assumptions of one-dimensional flow in the throat and at the exit of the duct as well as the assumption of atmospheric pressure at the exit.

The linearity of an incompressible potential flow model even for large pressure changes and high area ratios results in the fact that the complete behavior of a given shape can be investigated for all values of pressure drop across the actuator disk within a single calculation. The linearity also results in one obtaining the solution for vortex-panel strength from a simple matrix inversion. As will be seen, the downstream cylindrical vortex sheet is easily incorporated into this linear model. This solution may also prove useful as initial conditions for a more detailed CFD simulation.

Werle and Presz (2008) were the first to point out that the increased power from a ducted wind turbine as compared to the Betz model implied a force acting on the duct in the flow direction. Clearly in an inviscid potential flow this force is due to the pressure distribution acting on the duct, which can be resolved easily from an aerodynamic model of the flow within and outside of the duct. In their exposition, they assumed that the force on the duct was simply proportional to the pressure drop across the disk. This leads directly to a prediction of the augmentation of power by the duct that is simply related to the Betz power curve by a factor of proportionally, the maximum power occurring at the same value of velocity change in the far wake as in the Betz model.

However, as we shall show from our model, there are additional aerodynamic forces acting on the duct due to the interaction between the Kutta condition and the pressure drop across the disk. These additional forces are not proportional to the pressure drop across the disk and the resulting turbine power curve is not proportional to the Betz power curve. A dominant role is played by leading-edge suction. In essence, the Kutta condition determines how much of the flow goes through and how much goes around the duct. This creates a leading-edge suction on the airfoil/duct. This leading-edge suction creates a negative drag on the duct which when combined with the pressure drag on the airfoil surface due to the static pressure change across the disk, creates a total force on the duct which, when combined with the force on the actuator disk itself, will be shown to quite nicely balance the total momentum change in the flow.

Previous analysis of ducted turbines into two camps. In most cases the role of the Kutta condition has been ignored in favor of focusing on the internal flow, assuming atmospheric pressure and one-dimensional flow at the downstream edge of the duct. (See for example Jamieson (2008), Hansen (2000) and van Bussel (2007).) Again some cases, primarily in the analysis of ducted propellers, a form of Kutta condition was applied as described in Lewis (1991). We are unaware of a complete analysis of the total aerodynamic field of a ducted turbine with a proper balancing of momentum, calculation of forces on the duct, inclusion of the velocities induced by the vortex wake, and calculation of turbine efficiency for a given duct over a significant range of pressure drops.

The results of this simplified analysis answers some questions that have remained conjecture such as the power extracted by a ducted turbine in comparison to the Betz model, when the reference area is taken

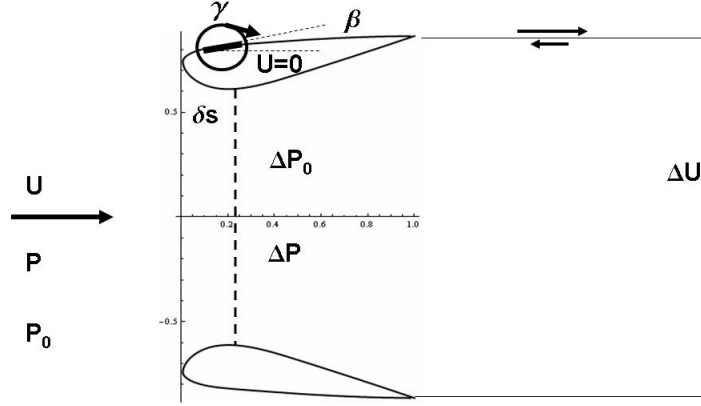


Figure 1: Geometry of Airfoil/Duct

as the outlet area. We shall show that when referred to the exit area the power obtained from a ducted turbine is essentially independent of throat area relative to exit area and lower than the Betz efficiency over a portion of the range.

Two- and Three-Dimensional Lifting Airfoils by Vortex Methods

Lewis (1991) pioneered the application of vortex methods to construct potential flow solutions for lifting airfoils for both two-dimensional and axisymmetric ducts. These methods are particularly appropriate for airfoil/ducts with thickness since the airfoil shapes are represented by vortex panels placed directly upon the airfoil/duct surface. The configuration studied is shown in Figure 1. In two-dimensions it consists of a pair of airfoils symmetrically placed about a center plane; in three dimensions it is an annular duct; in both cases the flow is parallel to the axis of symmetry. The coordinates of the actual airfoil appear in the appendix. The airfoil surface is replaced by a distribution of vortex panels of length δs aligned with the local slope. The angle β is defined as shown: the angle between the horizontal and the local panel alignment. Control points on the airfoil surface are taken from the lower surface at the trailing edge to the upper surface of the trailing edge in the clockwise direction as in Lewis. (100 control points were used for these calculations.)

The essence of Lewis's method is that the velocities due to the vortex panels, when combined with the free stream velocity, result in zero velocity *within* the airfoil boundary. Therefore, the value of γ is equal to the total velocity on the airfoil surface (or $-\gamma$ for the lower surface). For the airfoil/duct configuration in a free stream, the application of vortex methods is straightforward for both two-dimensional and axisymmetric flows. For a wind turbine or ducted propeller, an additional consideration must be given to the stagnation-pressure discontinuity across the actuator disk. This results in a velocity discontinuity—or vortex sheet—originating from the trailing edge of the airfoil/duct. It also gives rise to questions about the form of the Kutta condition to be applied.

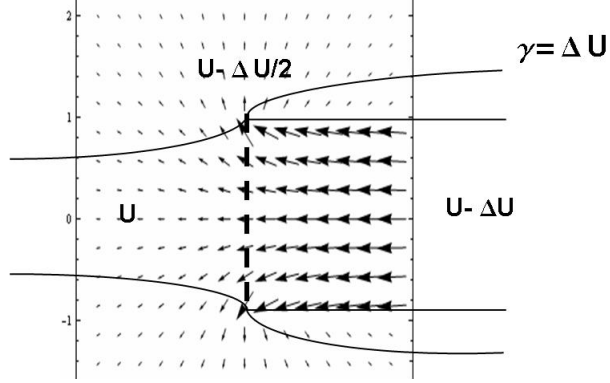


Figure 2: Flow Field of the Betz Model

Before considering these issue, we examine the "potential flow" solution to the Betz actuator-disk problem. Considerable insight into the Betz model and its relation to the present model can be obtained by considering the flow field from a semi-infinite vortex wake in either two- or three-dimensional flow as show in Figure 2. The total solution for the actuator disk problem is obtained by adding a free stream of velocity U to the vortex wake solution. (The form of these solutions is given in an appendix for both two-dimensional and axisymmetric flow.) In both cases, both the horizontal velocity U and the vertical velocity V are continuous- and irrotational- across the "disk". The U velocity in the far downstream wake is $U - \Delta U$. And the change in U velocity at the disk is uniform and exactly equal to $1/2$ of ΔU . Of some interest is that the vertical velocity V is not zero on the disk but has a logarithmic singularity near the upper edge. When this V velocity is integrated from $-\infty$ to $+\infty$, a good approximation for the shape of the Betz bounding streamline is obtained.

The vortex sheet experience a vertical self-induced velocity which will transport the sheet causing it to assume the proper curved shape. However, this effect should have little effect on the velocity field induced at the actuator disk. From this simple model, momentum change and power extraction can be calculated leading to the Betz model for wind turbine performance.

Two- and Three-Dimensional Flows with No Vortex Wake

The Lewis equations for airfoil/ducts without the presence of an actuator disk-and thus no trailing vortex sheet- are given by Equation 2.23 of Lewis.

$$\sum_{n=1}^M (K(s_m, s_n) + \delta s_m) \gamma_1(s_n) = -(U_\infty \cos \beta_m + V_\infty \sin \beta_m) \quad (1)$$

$$\sum_{n=1}^M (K(s_m, s_n) + \delta s_m) \gamma_2(s_n) = 1 \quad (2)$$

where $K(s_m, s_n)$ is called the coupling coefficient: the velocity parallel to the vortex panel m due to the vortex panel n ; and δs is the length of the panel. Various forms for the coupling coefficients are presented in

the appendix for both two- and three dimensional flow. For near-field effects, panels with constant vorticity are used; for far-field effects, a point vortex solution is used. Self-coupling must be carefully considered, particularly in three-dimensional flow where the curved vortex filament possesses a logarithmic singularity. These issues are discussed in Lewis. In our case, the free stream is in the U direction only.

From a physical point of view, the first equation requires a set of vortex panels γ_1 to cancel out the component of the free stream U_∞ that would otherwise cause a non-zero velocity inside the airfoil; the second equation requires a set of vortex panels γ_2 to cancel out the velocity inside the airfoil induced by the circulation around the airfoil. These insights will be important in taking the next step to include the presence of the vortex wake. In this calculation, we shall non-dimensionalize by taking the free stream velocity $U_\infty = 1$, and the free stream density as $\rho = 1$.

The solution is obtained by inversion of the matrix $(K(s_m, s_n) + \delta s_m)$, which is the same for both equations. The two γ distributions are then obtained by matrix multiplication. The combined solution is then

$$\gamma = \gamma_1 + \Gamma\gamma_2 \quad (3)$$

where Γ is the total bound circulation, which is unknown at this point. This is found from the Kutta condition; in this case the requirement that the pressure is continuous at the trailing edge reduces to the condition that the velocity is continuous at the trailing edge. Since by the definition of positive circulation, the velocities at the upper and lower surfaces of the trailing edge are given by

$$u_u(te) = \gamma(M) \quad (4)$$

$$u_l(te) = -\gamma(1) \quad (5)$$

where $n = 1$ is the element of the lower trailing edge and $n = M$ is the element of the upper trailing edge, resulting in

$$\Gamma = -\frac{\gamma_1(1) + \gamma_1(M)}{\gamma_2(1) + \gamma_2(M)} \quad (6)$$

in agreement with Equation (2.25) of Lewis, so that the solution is now complete. Calculations were done for two-dimensional flow and good agreement was obtained for the pressure distribution on a Karman Trefftz airfoil. Calculations were also done for the airfoil/duct shown in Figure 1 for three-dimensional flow for area ratios 2, 3, and 4. The results for velocity and pressure distributions were obtained. These will be presented and discussed with the full solution including the effect of the vortex wake. Satisfaction of the Kutta condition, equation (6) gives $\Gamma = -1.25$ for the duct of area ratio 2 with no actuator disk. (For the calculation of Γ , the airfoil chord was taken as unity.) For these calculations, M was taken as 100. The calculations were done using Mathematica.

Formulation: Annular Duct with Actuator Disk; Vortex Wake Included

The stage is now set for the introduction of the actuator disk, its accompanying vortex wake and its effect on flow field of the airfoil/duct. The focus is on the velocity field induced by the vortex wake and its inclusion

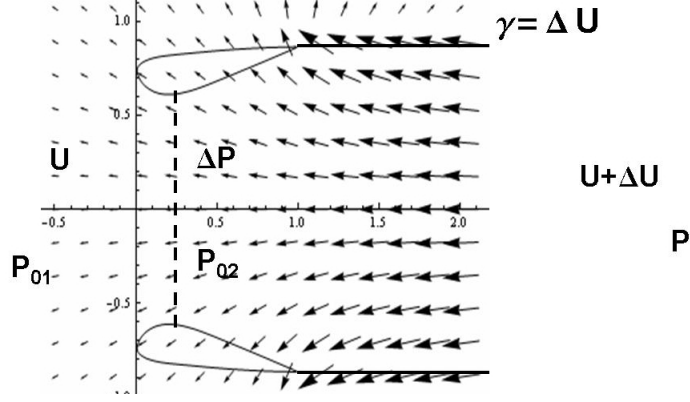


Figure 3: Flow Field and Geometry of Airfoil/Duct with Vortex Sheet

in the method of Lewis which incorporates an additional equation into the framework of Equations (1, 2). For a free stream velocity, $U_\infty = 1$, the velocity far downstream in the wake is given by $1 - \Delta$. The velocity field seen by the airfoil for the velocity change of $-\Delta$ is given by $U_w(x, y)$ and $V_w(x, y)$ (or x, r) as given in the appendix for both two- and three -dimensional flows.

Figure 3 shows the velocity field experienced by the duct as a result of the trailing vortex sheet. Since the airfoil is also a vortex sheet, the airfoil boundary condition will interact with the vorticity generated at the disk itself, resulting in a satisfaction of the airfoil boundary condition, leaving a "Betz" vortex wake beginning at the trailing edge.

The governing equations are then

$$\sum_{n=1}^M (K(s_m, s_n) + \delta s_m) \gamma_1(s_n) = -(U_\infty \cos \beta_m) \quad (7)$$

$$\sum_{n=1}^M (K(s_m, s_n) + \delta s_m) \gamma_2(s_n) = 1 \quad (8)$$

$$\sum_{n=1}^M (K(s_m, s_n) + \delta s_m) \gamma_3(s_n) = -(U_w(x, y) \cos \beta_m + V_w(x, y) \sin \beta_m) \quad (9)$$

The incorporation of the vortex wake is thus straightforward. The coupling matrix to be inverted remains the same as for a flow without a vortex wake and an additional vortex distribution γ_3 accounts for the effect of the wake. That is, γ_3 exists on the airfoil to prevent the velocities induced on the airfoil/duct by the vortex wake from violating the airfoil boundary condition.

Also for a given value of Δ , the value of the change in stagnation pressure $p_{01} - p_{02}$ across the disk is determined from Bernoulli's equation. The Kutta condition now becomes the requirement that the pressure is continuous at the trailing edge. For our non-dimensionalization of $U_\infty = 1$ and $\rho = 1$, Bernoulli's equation, the relation between the stagnation and static pressure drop across the disk and the strength of the vortex sheet Δ , is

$$p_{01} - p_{02} = p_1 - p_2 = \Delta - \Delta^2/2 \quad (10)$$

The velocities at the upper and lower trailing edge are

$$u_u(te) = (\gamma_1(M) + \Gamma\gamma_2(M) + \Delta\gamma_3(M)) \quad (11)$$

$$u_l(te) = -\gamma_1(1) - \Gamma\gamma_2(1) - \Delta\gamma_3(1) \quad (12)$$

and the Kutta condition of equal pressure at the training edge becomes

$$1/2(u_u(te)^2 - u_l(te)^2) = \Delta - \Delta^2/2 \quad (13)$$

Solution of this equation determines Γ (and therefore $\gamma_1(1)$, $\gamma_2(1)$, $\gamma_3(1)$, $\gamma_1(M)$, $\gamma_2(M)$, and $\gamma_3(M)$) as a function of Δ for a particular configuration.

For the present calculations for the annular duct of area ratio 2, the numerical result for Γ is

$$\Gamma = 2.58 \left(1.08 + 0.326\Delta - 0.78\sqrt{4 - 3.7\Delta + \Delta^2} \right) \quad (14)$$

which is in agreement with $\Gamma = -1.25$ for $\Delta = 0$. Although not obvious from the form of the equation, Γ is essentially linear over the range of interest. This will be compared subsequently with the direct integration of the numerical solution for duct circulation as a function of Δ .

Results

Calculations have been done for annular ducts of area ratio 2, 3, and 4 with an airfoil shape as shown in Figure 1. To obtain ducts of various area ratios, the airfoil shape was held constant and then displaced radially to obtain the desired area ratios. For each case, a variety of non-dimensional wake velocity changes $\Delta's$ ($U_{wake} = 1 - \Delta$) were examined from $\Delta = 0$ to $\Delta = .8$. Momentum loss and power extracted were calculated and compared with the Betz values for an actuator disk of the same area as the duct throat taken as unity. The upper and lower surface pressure distributions on the duct surface are shown in Figure 4 for a duct of area ratio 2 for a variety of $\Delta's$: 0,.2,.4,.6,.8; $\Delta = 0$ corresponds to the pressure distribution for an annular duct with no actuator disk. The pressure at the trailing edge, determined by satisfying the Kutta condition, was not equal to atmospheric although for this particular duct, it came quite close.

Of interest is the fact that the adverse pressure gradient in the duct decreases as increased power is extracted. This makes the design of a ducted wind turbine somewhat more achievable. The velocity distribution on the upper and lower surfaces for a variety of $\Delta's$ is shown in Figure 5. Apparent is the velocity discontinuity at the trailing edge.

As would be expected for a two-dimensional/three-dimensional potential flow, the u velocity at the throat is not constant with radius. Figure (6) shows the non-dimensional velocity profiles as a function of non-dimensional radial distance r/r_{MAX} for ducts of area ratio 2, 3, and 4 for Δ ranging from 0 to .8. The variation in velocity across the duct throat decreases with increasing Δ . The variation in $U(r/r_{MAX})$ is larger for area ratio 2 than for area ratio 4.

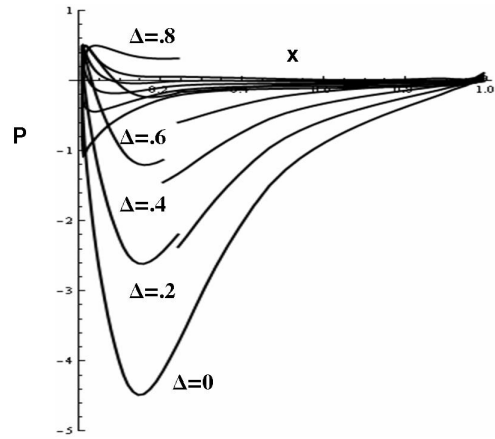


Figure 4: Pressure Distribution on the Duct Surface for Various Values of Δ

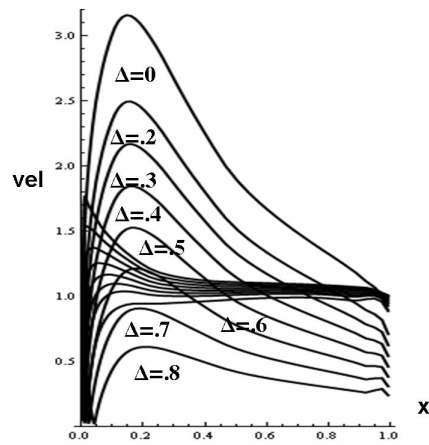


Figure 5: Velocity Distribution on the Duct Surface for Various Values of Δ

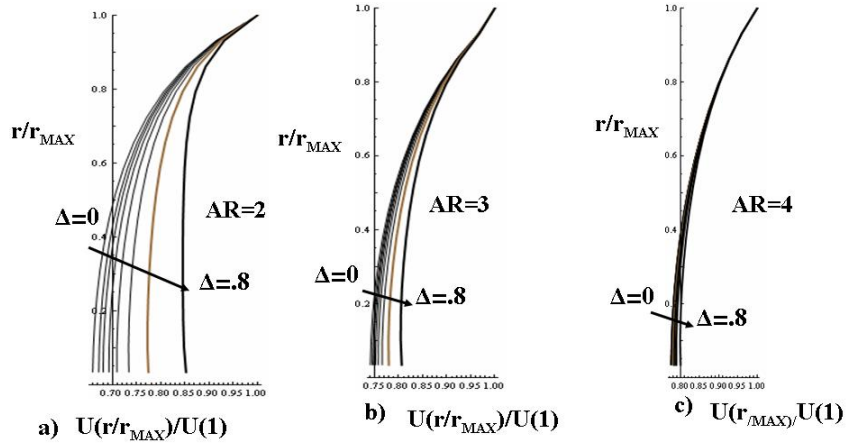


Figure 6: Velocity Profiles Across the Duct Throat

The total mass flow was calculated by integrating these profiles for each case. Calculation of the mass flow leads directly to momentum flow since the momentum extracted per unit mass (or volume for $\rho = 1$) is a function only of Δ ; the results are shown in Figure 7. As expected, the mass flow decreases as the pressure drop increases. Its linear behavior is perhaps surprising. As the momentum loss per unit mass increases with Δ , the mass flow through the duct decreases. The net result is the momentum loss as a function of Δ shown on Figure 8.

Figure 8 shows the momentum loss in the flow for both the Betz isolated actuator disk and the ducted configuration for area ratio 2. The momentum loss is referred to a unit throat area. The increased momentum

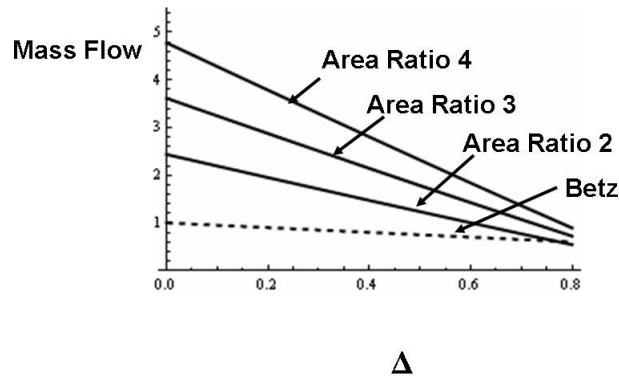


Figure 7: Mass Flow as a Function of Δ

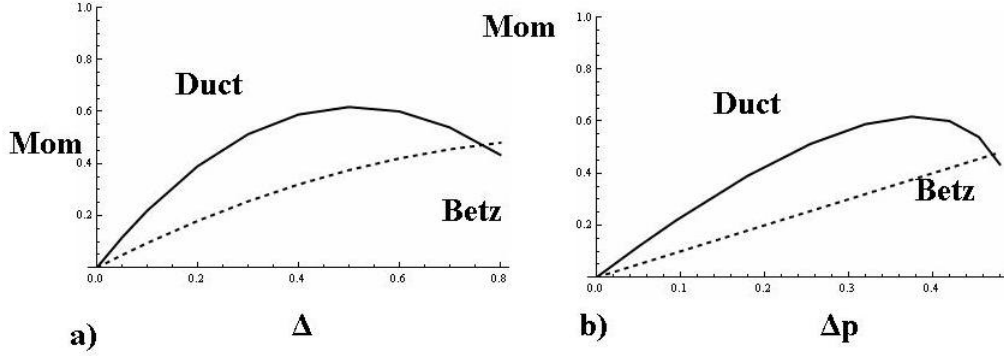


Figure 8: Momentum Loss the Flow for the Duct and the Betz Model

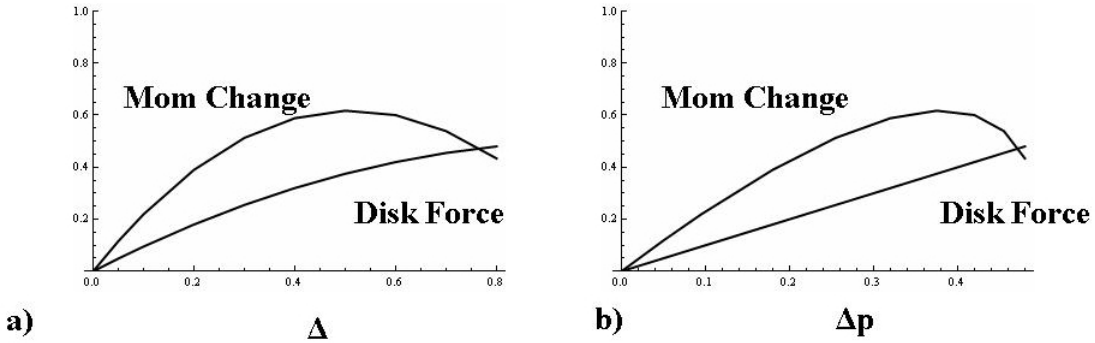


Figure 9: Momentum Loss in the Flow and Pressure Force on the Actuator Disk: a) vs Δ ; b) vs. Δp

loss in the ducted flow is evident. For convenience in comparing to previous analytical results and to experiments, the results are shown plotted against both the non-dimensional wake-velocity change Δ and the pressure change across the actuator disk Δp . From Bernoulli's equation, $\Delta p = \Delta - \Delta^2/2$.

Shown in Figure 9 is the momentum loss in the ducted flow and the force acting on the actuator disk referred to a unit throat area (which is also equal to the momentum extracted by an isolated actuator disk in the Betz model); they do not balance. It is clear that an additional force must act on the duct to balance this increased momentum loss. The momentum loss and the force on the actuator disk are plotted vs the change in non-dimensional velocity in the wake, Δ in a) and vs. the change in static/stagnation pressure across the actuator disk, Δp in b).

Calculation of Circulation, "Lift" and Drag on the Duct

We now calculate the net pressure forces acting on the duct. The "lift" force is not really lift, but is a suction pressure directed towards the origin. We have already determined Γ from the satisfaction of the Kutta condition; we now calculate it directly from surface pressure integrals.

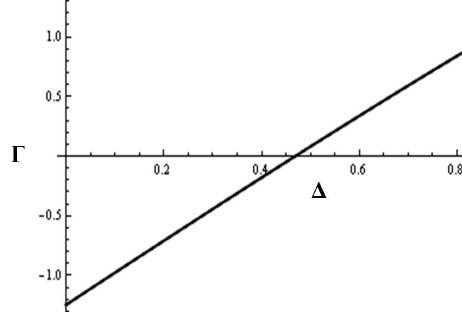


Figure 10: Duct Circulation

Circulation is calculated from

$$\Gamma = \oint \gamma(s) ds \quad (15)$$

where $\gamma(s)$ is the total value of the strength of a vortex panel at a point s on the surface as a function of Δ , after satisfying the Kutta condition. The direct calculation of Γ shown in Figure 10 agrees with the result of Equation (14) obtained by satisfying the Kutta condition of equal pressures at the trailing edge. This is compared numerically with Equation (14); the results are indistinguishable.

The "lift" and drag are calculate by direct integration of the pressure. The pressure distribution on the airfoil has two components: that related to the vorticity distribution $\gamma(s)$; and that related to the stagnation pressure drop through the screen, given by $\Delta - \Delta^2/2$,

$$lift(\Delta) = - \oint 1/2(1 - \gamma(s)^2) dx * 2 * \pi * r(x) + \int (\Delta - \Delta^2/2) * dx * 2 * \pi * r(x) \quad (16)$$

$$drag(\Delta) = \oint 1/2(1 - \gamma(s)^2) dr * 2 * \pi * r(x) - \int (\Delta - \Delta^2/2) * dr * 2 * \pi * r(x) \quad (17)$$

where the integral in the second term is taken only over that portion of the airfoil where the stagnation pressure has changed. The term $2\pi r(x)$ accounts for the circumferential area of the duct in carrying out the area integral. The integral is calculated numerically in the clockwise direction using the solution determined at the control points.

Of considerable interest are the results for drag shown in Figure 11. Shown is the drag due to the pressure deficit on the rearward facing duct sections. Also shown is the leading edge suction which for the most part contributes a negative drag. The the sum is the total pressure drag, also shown. Forces are calculated for a duct of unit throat area. The total drag and the various drag components are plotted vs. Δ in a) and vs. Δp in b).

The various components of the force and momentum are shown in Figure (12). Shown are the total longitudinal force on the duct/turbine combination, which is the sum of the pressure force on the actuator disk (shown) and the total drag force on the airfoil/duct (shown).

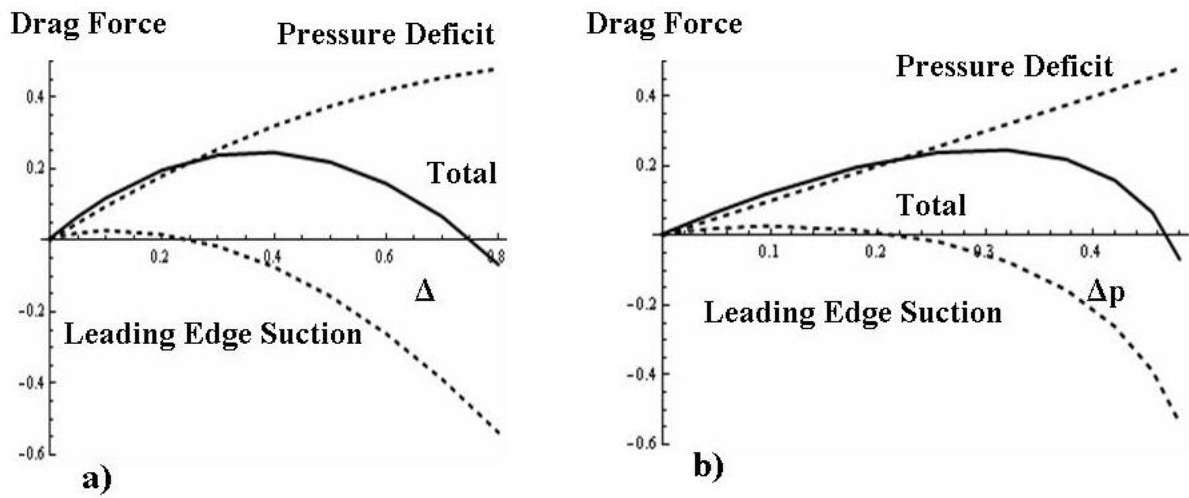


Figure 11: Drag Components and Total Drag

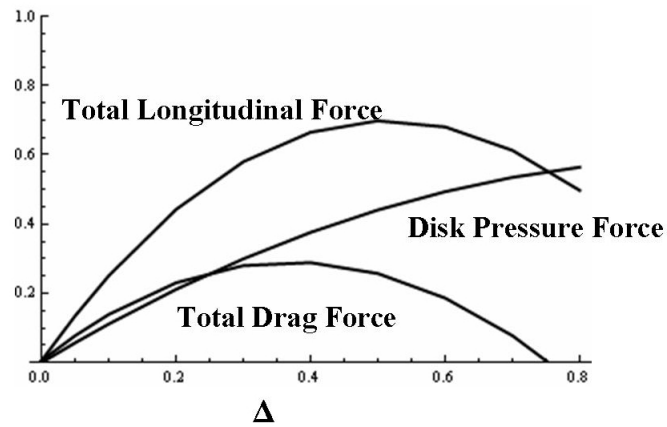


Figure 12: Balance of Flow Momentum and Total Drag Force

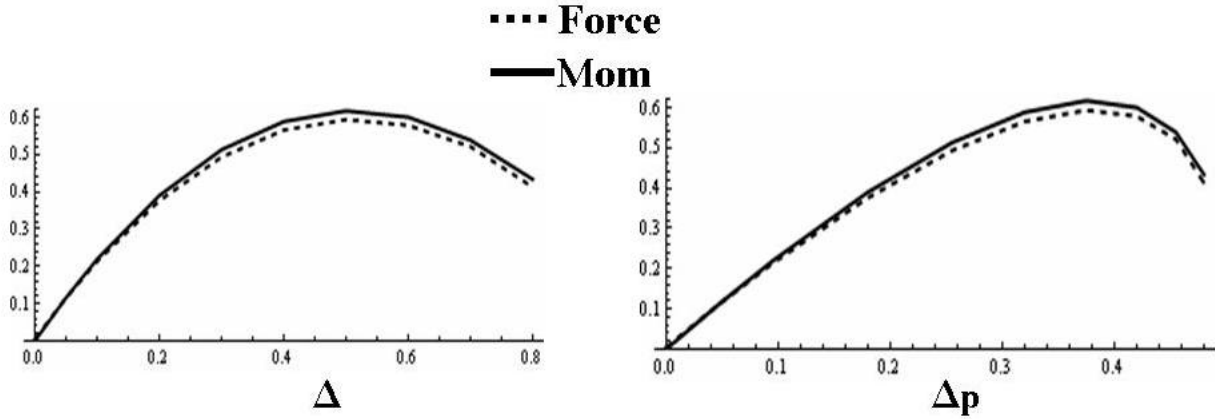


Figure 13: Balance of Flow Momentum and Total Drag Force

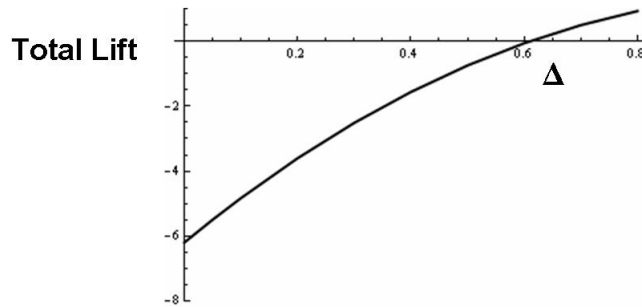


Figure 14: Total "Lift" on Duct Sections

The resulting total force balances the momentum loss from Figure (9) as shown in Figure (13): the force/momentum balance is plotted against both Δ in a) and Δp in b).

Questions remain about the application of potential flow to a ducted turbine modeled as an actuator disk or to an experiment in which uniform screens are used to model the disk, since it is unlikely that the pressure drop across the actuator disk would be constant with a non-uniform flow entering the disk. However, this modeling defect is related to many of the issues in modeling a wind turbine by an actuator disk. Even in the face of this, the potential flow gives useful insights and valuable results.

The total "lift" was also calculated, as shown in Figure 14. It is of less interest since it is not really lift, but a suction force on the airfoil sections of the duct directed towards the centerline producing no net force on the duct.

Now that momentum has been balanced, we turn our attention to power extracted. Figure (15) shows the power extracted by a ducted turbine in a duct of area ratio 2 and an isolated actuator disk, both of unit area; the results are plotted against Δ in a) and Δp in b). The power results show that the maximum power occurs at lower values of the vortex sheet strength Δ and/or Δp , the pressure change across the actuator

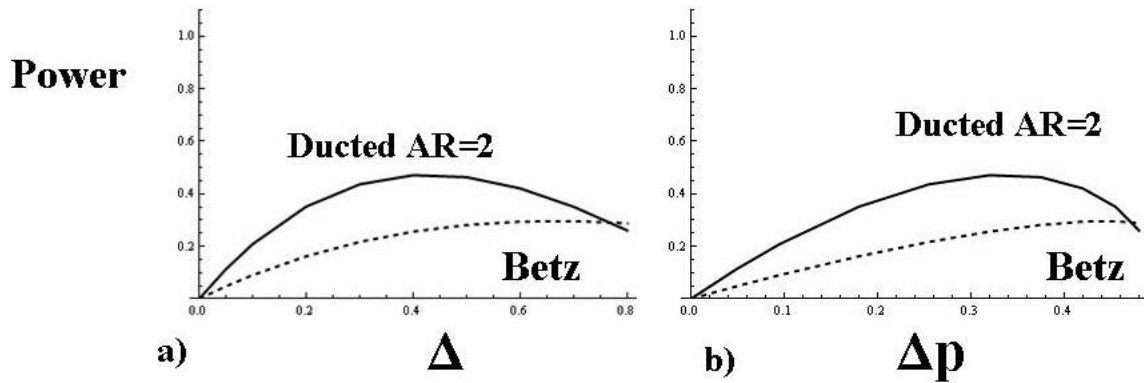


Figure 15: Total Power: Ducted Wind Turbine and Betz Model

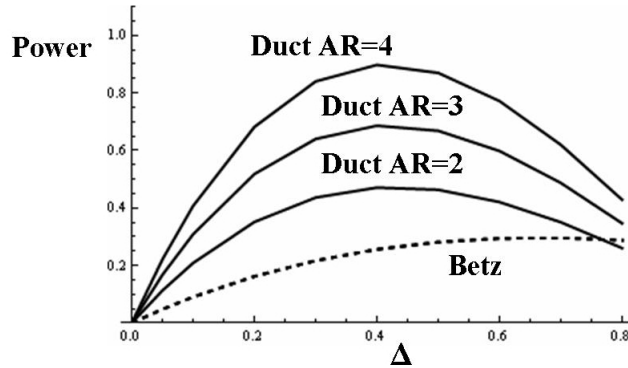


Figure 16: Total Power: Ducted Wind Turbine and Betz Model For Area Ratio 2, 3, and 4 (unit throat area).

disk than for an actuator disk turbine in a free stream. The corresponding results for wind turbines in ducts of area ratios 2, 3, and 4 (with unit throat area) are shown in figure (16). The results for area ratio 4 are perhaps of academic interest only since it is unlikely that in a viscous flow that the strong adverse pressure gradients in such a duct could be overcome. However, as the power extraction increases, the magnitude of the adverse pressure gradients decreases, making the flow somewhat more achievable. None-the-less, these results are useful as a benchmark.

It has been argued that, if the power extraction of a ducted turbine as compared to the Betz model is referred to the exit area of the duct rather than the throat area, no power augmentation occurs (For example van Bussel (2007)). Numerical confirmation of this hypothesis can be seen in Figure (17) which shows the power extracted referred to the exit area. This result shows that the power extracted does not exceed the Betz limit when referred to the exit area and is rather insensitive to the duct area ratio. It also shows that the maximum power extraction for a ducted turbine occurs at a lower value of Δ than that of the Betz turbine and that the power extracted by an isolated turbine according to the Betz model exceeds that of the ducted

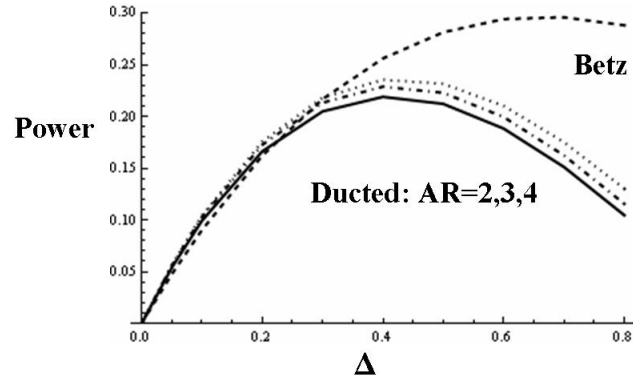


Figure 17: Total Power: Ducted Wind Turbine and Betz Model For Area Ratio 2, 3, and 4 referred to Exit area.

turbine over a substantial portion of its operating range. The application of these results to a given design depends upon whether the economies relate to the size of the wind turbine or to the size of the duct.

Appendix: Vortex Flow Fields

Two-Dimensional Vortex Flow Fields

The fundamental singularity in Lewis's method is the vortex panel. As a basic element, we consider a two-dimensional vortex panel of length $2a$ symmetrically placed about the point $x - x_0$ and $y - y_0$, and tipped at an angle θ_0 as shown in Figure (18a),

the u and v velocities at the points x, y are given by

$$\begin{aligned}
u(x - x_0, y - y_0, \theta_0) = & \\
& \frac{1}{2\pi} \left(\arctan \left[\frac{a + (x - x_0) \cos \theta_0 - (y - y_0) \sin \theta_0}{(y - y_0) \cos \theta_0 + (x - x_0) \sin \theta_0} \right] \right) \cos \theta_0 \\
& + \frac{1}{2\pi} \left(\arctan \left[\frac{a - (x - x_0) \cos \theta_0 + (y - y_0) \sin \theta_0}{(y - y_0) \cos \theta_0 + (x - x_0) \sin \theta_0} \right] \right) \cos \theta_0 \\
& + \frac{1}{4\pi} \left(-\log \left[((y - y_0) \cos \theta_0 + (x - x_0) \sin \theta_0)^2 + (a + (x - x_0) \cos \theta_0 - (y - y_0) \sin \theta_0)^2 \right] \right) \sin \theta_0 \\
& + \frac{1}{4\pi} \left(\log \left[((y - y_0) \cos \theta_0 + (x - x_0) \sin \theta_0)^2 + (a - (x - x_0) \cos \theta_0 + (y - y_0) \sin \theta_0)^2 \right] \right) \sin \theta_0 \\
v(x - x_0, y - y_0, \theta_0) = & \\
& \frac{1}{4\pi} \cos \theta_0 \left(-\log \left[((y - y_0) \cos \theta_0 + (x - x_0) \sin \theta_0)^2 + (a + (x - x_0) \cos \theta_0 - (y - y_0) \sin \theta_0)^2 \right] \right) \\
& + \frac{1}{4\pi} \cos \theta_0 \left(\log \left[((y - y_0) \cos \theta_0 + (x - x_0) \sin \theta_0)^2 + (a - (x - x_0) \cos \theta_0 + (y - y_0) \sin \theta_0)^2 \right] \right) \\
& - \frac{1}{2\pi} \left(\arctan \left[\frac{a + (x - x_0) \cos \theta_0 - (y - y_0) \sin \theta_0}{(y - y_0) \cos \theta_0 + (x - x_0) \sin \theta_0} \right] \right) \sin \theta_0 \\
& - \frac{1}{2\pi} \left(\arctan \left[\frac{a - (x - x_0) \cos \theta_0 + (y - y_0) \sin \theta_0}{(y - y_0) \cos \theta_0 + (x - x_0) \sin \theta_0} \right] \right) \sin \theta_0
\end{aligned} \tag{18}$$

For $x - x_0$ and $y - y_0$ greater than say $3a$, this flow field may be approximated by a point vortex of strength $2a$ located at the point x_0, y_0 .

$$u_v(x - x_0, y - y_0) = \frac{2a}{2\pi} \frac{(y - y_0)}{(x - x_0)^2 + (y - y_0)^2} \tag{19}$$

$$v_v(x - x_0, y - y_0) = \frac{-2a}{2\pi} \frac{(x - x_0)}{(x - x_0)^2 + (y - y_0)^2} \tag{20}$$

In preparation for the construction of a three-dimensional axisymmetric wake vortex sheet, vortex panel and point vortex flow, we construct a semi-infinite vortex wake of unit strength in two dimensions as sketched in Figure (18g), initiated at the point $x = 1$ and $y - y_0$, and reflected about $y = 0$; this flow has a velocity field given by

$$U_w(x, y) = -\frac{1}{2\pi} (\arctan(y - y_0/x - 1) - \arctan(y - y_0/x - 1)) \tag{21}$$

$$V_w(x, y) = -\frac{1}{4\pi} \log \frac{(x - 1)^2 + (y - y_0)^2}{(x - 1)^2 + (y + y_0)^2} \tag{22}$$

From this flow field, a finite vortex panel including its reflection about $y = 0$ may be constructed by beginning a semi-infinite vortex wake and then subtracting a displaced wake of opposite sign separated by a distance $2a$ as sketched in Figure (18h). This gives the formula for a two-dimensional vortex panel of $2a$ located at $x = 0, y = y_0$ aligned in the x direction with a reflected panel at $y = -y_0$. The horizontal panel can be obtained from equation (18) by setting $\theta_0 = 0$. We will later use this technique to construct a vortex panel in three-dimensional axisymmetric flow. As discussed in Lewis, numerical results are sensitive to the mutual

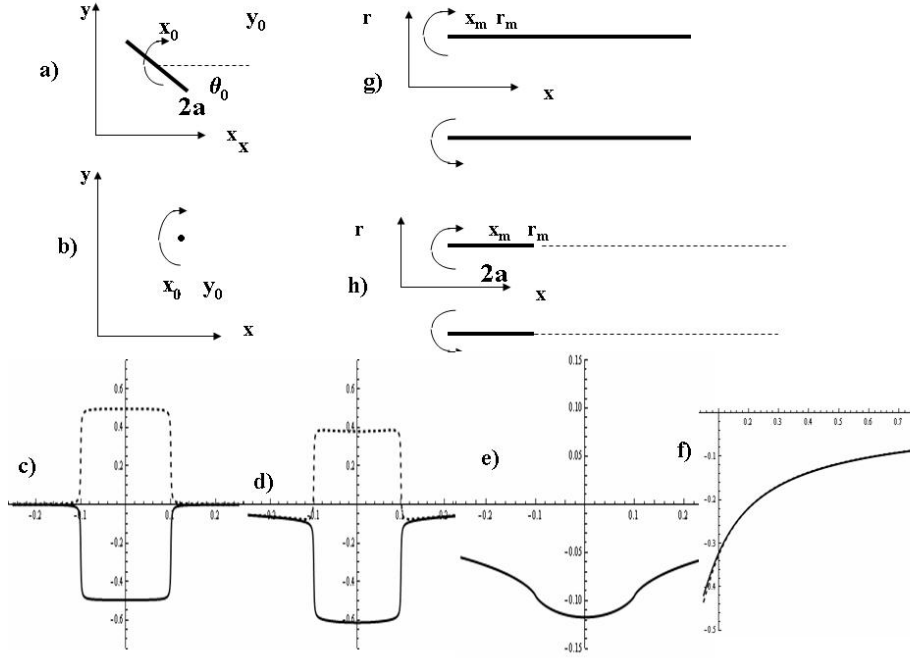


Figure 18: Vortex Geometry for panel, wake and point.

influence of vortex singularities of nearby panels. Therefore in regions such as the trailing edge where panels are close on opposing sides, it is important to provide an accurate representation of the flow field. The use of vortex panels of constant strength accomplishes this. The velocity field of a single two-dimensional horizontal vortex panel is given by

$$v_{p2D} = -\frac{1}{2\pi} \left(\frac{1}{2} (\log((a-x)^2 + y^2) - \log((a+x)^2 + y^2)) \right) \quad (23)$$

$$u_{p2D} = \frac{1}{2\pi} (\arctan[(x-a)/y] - \arctan[(x+a)/y]) \quad (24)$$

Three-Dimensional Vortex Flow Fields

Many of the three-dimensional vortex field formulae are given in Lewis. The equivalent expression of a point vortex –which in this case is a vortex ring– is given by equation (4.8-4.11). The vortex ring is of radius r_n located at $x = x_n$; the velocity field is evaluated at $x = x_m$ and $r = r_m$

$$u_{x3D} = \frac{-2a}{2\pi r_n \sqrt{(X^2 + (R+1)^2)}} (K(k) - ((1 + \frac{2(R-1)}{X^2 + (R-1)^2})E(k))) \quad (25)$$

$$u_{r3D} = \frac{2a(X/R)}{2\pi r_n \sqrt{(X^2 + (R+1)^2)}} (K(k) - ((1 + \frac{2R}{X^2 + (R-1)^2})E(k))) \quad (26)$$

where $X = (x_m - x_n)/r_n$, $R = r_m/r_n$ and $k = \sqrt{\frac{4R}{X^2 + (R+1)^2}}$. X and R are non-dimensional coordinates; k is the argument of the Elliptic functions of the first and second kind $K(k)$ and $E(k)$.

Lewis also give the corresponding expressions for the semi-infinite vortex wake/tube located at $x = x_n$, $r = r_n$. For a velocity change across the vortex sheet of $-\Delta$, the wake velocities are given by

$$U_w(X, R) = \frac{-\Delta}{(2\pi)} \left(A + \frac{X}{(\sqrt{X^2 + (R+1)^2})} (\mathbf{K}(k) - \frac{(R-1)}{(R+1)} \Pi(n, k)) \right) \quad (27)$$

$$V_w(X, R) = \frac{2\Delta}{(\pi k^2 \sqrt{X^2 + (R+1)^2})} (\mathbf{E}(k) - (1 - \frac{k^2}{2}) \mathbf{K}(k)) \quad (28)$$

where $X(x_m, x_n, r_n)$ and $R(r_m, r_n)$ are non-dimensional coordinates previously defined. $\Pi(n, k)$ is the complete Elliptic integral of the third kind; and $A = \pi$ if $r < 1$; $A = \pi/2$ if $r = 1$; and $A = 0$ if $r > 1$. The arguments X and R are functions of the wake position x_n and r_n and the field points x_m, r_m : $X = X(x_m, x_n, r_n)$; $R = R(r_m, r_n)$ previously defined. To construct a three-dimensional vortex panel of radius r_n centered at x_n , we begin a wake of unit strength ($\Delta = 1$) at $x_n - a, r_n$ and add a wake of negative unit strength ($\Delta = -1$) at $x_n + a$ and r_n , thus canceling the downstream vortex component leaving a three-dimensional vortex panel of total strength $\gamma = 2a$. This process is sketched in Figure (18h). We denote this symbolically as

$$u_{p3D} = U_w(X(x_n - a, r_n)) - U_w(X(x_n + a, r_n)) \quad (29)$$

$$v_{p3D} = V_w(X(x_n - a, r_n)) - V_w(X(x_n + a, r_n)) \quad (30)$$

We now compare the numerical results for the velocity field induced by a vortex panel in two-and three dimensions. The velocity discontinuity across the two-dimensional vortex panel shown in Figure (18c) is 1, with $\pm 1/2$ on either side. The velocity discontinuity across the three-dimensional vortex panel shown in Figure (18d) is also 1, however the logarithmic singularity, when integrated across the panel, gives an additional velocity above and below the panel. This three dimensional effect is discussed in Lewis. In our three-dimensions calculation we account for this effect by constructing a near field panel solution which is the summation of a tipped two-dimensional panel plus a flat three-dimensional panel with a flat two-dimensional panel subtracted. This gives a proper accounting for the local geometry and the three-dimensional effects. For the far field, a simple three-dimensional point vortex ring is used.

Direct numerical calculations of the velocity field of a tipped three-dimensional vortex panel shows that this representation is quite accurate. However, the use of analytic representations rather than direct numerical integration results in considerable computational efficiency.

Airfoil Coordinates

The XAA and RAA coordinate of the airfoils used to form the duct in the present calculations is given in Figure (19). To form a duct of given area ratio, the airfoil was displaced in the radial direction to form an annular duct of a given area ratio, defined as $Area_{EXIT}/Area_{THROAT}$. Calculations were done for area ratios 2,3 and 4 (actually 4.1).

References

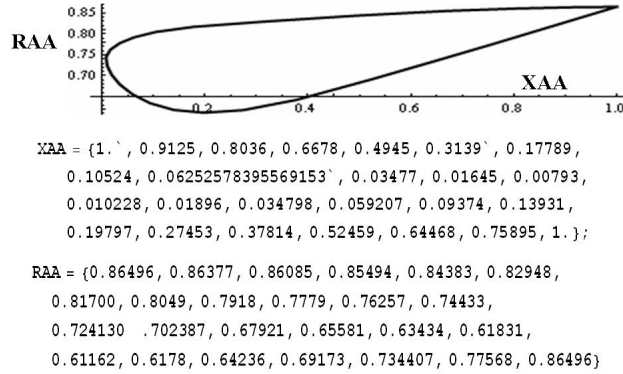


Figure 19: Airfoil Coordinates

Hansen, M.O.L. et. al., Effect of Placing Diffuser around a Wind Turbine, *Wind Energ.* 2000; 3:207-213

Jamieson, P., Generalized Limits for Energy Extraction in a Linear Constant Velocity Field, *Wind Energ.* 2008;11:445-457

Jamieson, P. Beating Betz-Energy Extraction Limits in a Uniform Flow Filed, *unpublished*; peter.jamieson@garradhassan.com

Lewis, R.I., Vortex Element Methods for Fluid Dynamic Analysis of Engineering Systems, Cambridge Engine Technology, Cambridge University Press 1991

Werle, M.J. and Presz Jr., W.M., Ducted Wind/Water Turbines and Propellers Revisited, *Journal of Propulsion and Power*, Vol. 24, No. 5, September-October 2008, 5th

Van Bussel, G.J.W., The Science of Making More torque from Wind: Diffuser Experiments and Theory Revisited, *Journal of Physics: Conference Series* 75 (2007) 012010